

Analysis of the Joint Effect of Heat Treatments and Stress Ratio on the Growth Behavior of Fatigue Cracks in Cast Aluminum Alloys under Combined Loading (Bending-Torsion)



Mustafa Sami Abdullatef^{*✉}, Anees Al-Tamimi[✉], Faten N. Alzubaidi[✉], Yasser Ahmed Mahmood[✉]

Electro-mechanical Engineering Department, University of Technology-Iraq, Baghdad P.B. BO 19006, Iraq

Corresponding Author Email: 50118@uotechnology.edu.iq

<https://doi.org/10.18280/rcma.330202>

ABSTRACT

Received: 1 February 2023

Accepted: 12 April 2023

Keywords:

fatigue, short and long cracks, combined loading, cast aluminum alloys, stress ratio, crack initiation, crack propagation, underaged and overaged microstructure

The behavior of microstructural short fatigue cracks (20-100 μm in length on the same scale as the grain size) in the cast aluminum alloy A07710-T6 was investigated. Two heat treatment conditions have been used, an underaged and an overaged microstructure, chosen to have very similar tensile properties, so that the effects of precipitation and hence slip distribution on fatigue behavior could be studied at the same strength level. The results of short crack propagation tests performed on smooth specimens at 25°C and $R=0.1$ are compared to conventional (long) fatigue crack propagation and threshold results under the same conditions. The short crack data is also compared to long crack tests conducted at constant maximum applied load (so that the R -ratio increases to a value above 0.8 as the threshold is approached). In conventional long crack tests, better low and high threshold crack propagation resistance is associated with the underaged microstructure. This behavior is also reflected in the thresholds obtained at high R .

1. INTRODUCTION

A material's ability to resist the development of fatigue cracks is influenced by a number of variables, including its composition, mechanical characteristics, and heat treatment settings, as well as external loads and the environment. Using theoretical techniques based on solid mechanics and fundamental mechanical properties, a number of theoretical models have been put forth to anticipate the fatigue crack growth (FCG) process. Quantitative understanding of the growth characteristics of brief fatigue cracks is crucial in order to accurately predict the fatigue life of a material and prevent the unanticipated catastrophic failure of an engineering structure as a result of fatigue damage. Due to the fact that a short fatigue crack's expansion may account for 50% to 90% of the fatigue life [1]. Previous studies have shown that the microstructural features of an engineering alloy, such as second phase particles, grain boundaries, and grain orientation, greatly influence the fatigue properties, particularly during the initiation and early propagation of tiny fatigue cracks. For a significant amount of a component's lifespan under cyclic loading, fatigue cracks frequently appear. As a result, any parameter that significantly influences the development of stress cracks may also have a considerable effect on the components' overall fatigue behavior. The stress ratio is one of these variables (ratio of minimum stress to maximum stress). The correlation of the parameters of fatigue crack growth rate, cyclic stress, and crack length has been successfully accomplished using the Paris relation, as is well known. This relationship is successfully extended in some situations to characterize the impact of the stress ratio R on the rate of fatigue crack growth for stages near the lower end of the Paris region [2].

2. FORMULATION OF THE FATIGUE CRACK GROWTH MODEL

In the past, it was suggested to utilize the stress intensity factor range as a metric to characterize how fatigue cracks expand. Later, it was discovered that the maximum stress severity factor plus the stress severity factor range controls FCG. There has not been much work done to establish a quantitative relationship between local stresses and stresses around the fracture tip and applied stress intensity parameters, despite the fact that they are the dominant factors in FCG.

Additionally, it was necessary to take into account the fact that the actual correlation was significantly impacted by the residual tension that the cyclic plastic deformation at the fracture tip caused. The monotonic plastic zone shown in Figure 1c is a result of the material near the fracture tip being deformed plastically during the initial loading reversal or the first nominal stress reversal from 0 to 1 (Figure 1a). The fracture tip deformations developed during the cycle's unloading phase (lines 1-5 in Figure 1a) are less severe than those produced during the preceding loading reversal. The plastic zone created during loading cannot disappear as a result, and a little portion of it is deformed once more in the opposite direction. The cyclic plastic zone refers to this re-deformed the plastic zone area (as shown in Figure 1c and load level 5). This distorted plastically substance acts as a barrier for upcoming reversals near the fracture tip. The material is plastically distorted, preventing closure of the area behind the fracture tip. In other words, even when compressive loads are applied, although not precisely behind the fracture tip, the surfaces of the fatigue crack do make touch with one another[3].

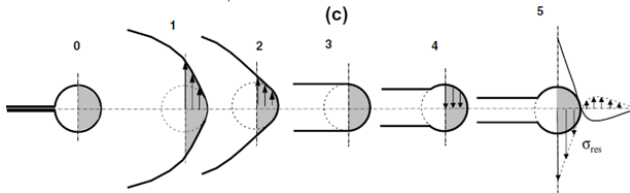
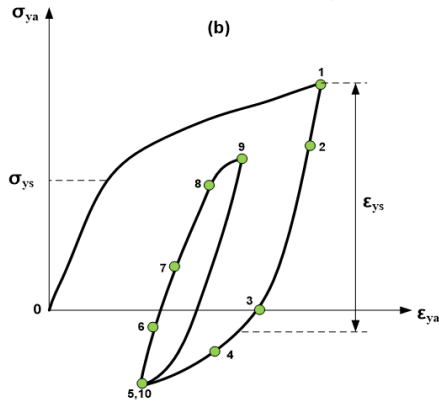
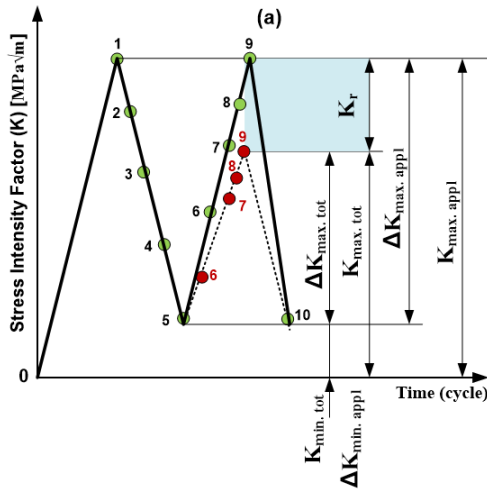


Figure 1. Crack tip stress-strain response, cyclic plastic zone, crack tip shape, and residual stress distribution: (a) the history of the applied load (stress intensity factor), (b) the crack tip's qualitative stress-strain response, (c) the evolution of the crack opening displacements there [3]

While a material is subjected to monotonic, quasi-static loading (K_{IC} when under mode I loading), the commencement of crack advance may occur if K is greater than the critical value of the stress intensity factor K_c . Later, under cyclic loading conditions, Paris, Gomez, and Anderson established a relationship between the range of K under cyclic loading with constant amplitude and the increment of da/dN , which is now popularly known as the Paris equation:

$$\frac{da}{dN} = C \cdot \Delta K^m \quad (1)$$

The crack formation mechanism is significantly more intricate than this equation can possibly express [4]. The red curve in Figure 2 shows the typical growth rate of a long fatigue fracture as a function of its stress intensity factor range at constant amplitude of cyclic loadings. This curve can be separated into three regions: region I: no propagation of fractures below a threshold value of K (however short fatigue cracks exhibit abnormal growth characteristics below $\Delta K_{threshold}$); region II: where $\log(da/dN)$ is directly

proportional to $\log \Delta K$, steady crack formation. Region III: unstable growth of crack. Paris equation solely explains region II of the propagation phase of a long fatigue crack [3].

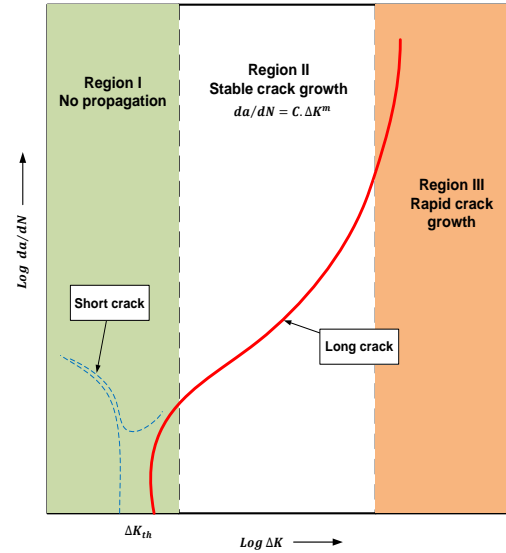


Figure 2. A typical fatigue fracture growing behavior under cyclic stress with constant amplitude [4]

Much research on fatigue crack growth (FCG) in alloys has been published, addressing several aspects of factors influencing short to long system crack growth and the importance of FCG thresholds. Wanhill and Stanzl-Tschegg [5], this study covers the fatigue design approaches for steam turbine LP blades and airframes in more depth. This includes the significance of environmental impacts, short fatigue cracks, fatigue crack development thresholds, high-cycle fatigue (HCF), and very-high cycle fatigue (VHCF) (corrosion and corrosion fatigue). Regarding design specifications, life estimations, and assessments, this report may be of interest to other researchers studying metal fatigue.

Spangenberg et al. [6], in this paper, loading microstructure damage processes design maps were generated in order to identify the mechanisms of long and small fatigue crack formation at the microstructural scale of the examined alloys. A novel fracture mechanics and materials science combination model was constructed, featuring both material and crack size dependency, to account for the differences in FCG responses between long, physically small, and microstructurally small cracks. Yoshinaka et al. [7] proposed in this work to conduct fatigue micro-crack propagation tests on Ti-6Al-4V in ultra-high vacuum, air, and argon. In order to understand the impacts of vacuum on crack propagation processes in comparison to air, the crack propagation rate in vacuum was significantly reduced. In the case of a small fracture system, the rate of crack propagation in argon is comparable to that of air; however, in the case of a long crack system, it resembles that of a vacuum. This shows that even in a chemically inert micro-crack system, the presence of gases has substantial impact. These findings led to the conclusion that the inhibitory influence of vacuum on small crack propagation is significantly inhibited by the absence of physical adsorption in addition to chemical inertness.

Wang et al. [8] examined the impact of grain boundaries on the development of fatigue cracks in the material 7050 – T7451 using the small time scale approach. Testing with an in situ SEM system confirmed the relationship between fatigue

crack and grain limitation. The findings demonstrated that when the angle between the fatigue fracture and the grain boundary is more than 90°, the grain boundaries will retard the formation of the fatigue crack. The results show that the bridge-joining mechanism caused the unstable fatigue crack propagation behavior that was frequently seen when the alloy experienced fatigue with constant capacity. In this study, Liu et al. [9] found electron backscattering diffraction and electron channel contrast imaging techniques were used to investigate the crack formation process and associated fatigue damage at the microstructure scale. The findings demonstrate that both the local microstructure and the overall force gradient have an impact on the short crack growth. Due to misfit deformation and strain localization, when the short fracture collides with one large grain, it may deflect intergranularly. The crack closure, which was accompanied by crack surface contact during loading and unloading, protected the true crack-tip and was clearly visible in both compressive strains at the crack wake and strain growth at the crack-tip.

Abdullatef [10], in his work artificially aged duralumin 7075-T6 underwent stress-controlled fatigue tests (under rotational bending load) for 70 hours in two different scenarios: case (1) without chemical treatment, case (2) with chemical treatment. Using a plastic replication technique, the growth behavior of short fractures was tracked, and optical microscopy was used to spot surface damage (short crack propagation) caused by cyclic loading. The beginning and growth behavior of short cracks were discussed in relation to the physical background of fatigue damage for cases (1) and (2). Pradhan et al. [11], in their present study, demonstrated the effect of average stress on IN718 superalloy for high cycle fatigue behavior at temperatures of 400, 500 and 600°C and strain rates (R) of 1, 0.5 and 0.7. As the average tensile stress increases, the fatigue life decreases. Multiple crack initiation sites on the sample surface are associated with reduced fatigue life at high average stress. Since the maximum stress approaches the yield stress and leads to cyclic ratcheting, the average tensile stress and the stress ratio, $R = 0.7$, have a significant effect on the fatigue limit.

In order to determine the significance of the stress ratio, Feng et al. [12] used in this study the test results on the stress crack propagation rate of TiAl alloys under different strain ratios to derive an optimized formula for stress crack propagation in the second region (expansion zone) according to the Paris equation and to determine the exact values of the formula constants. According to the results of the experiment, the stress ratio significantly affects the formation rate of fatigue cracks. After solution treatment, quenching, and three different artificial aging treatments, including two-step aging that leads to peak affinity state, one-step aging that leads to peak age, and three-step aging that leads to peak aging and fatigue. Desmukh et al. [13] studied the behavior of commercial Al 7010 alloy in the form of sheets with a thickness of 15 mm. The study shows that the fatigue crack

development rate (FCGR) of materials at their peak ages is the lowest, while those with older ages are the highest. However, the limiting value of stress crack propagation is larger in older materials. It is developed in materials that have undergone different aging processes.

The study of Li et al. [14] has looked at the fatigue-crack growth of the die-forged Al-5.87Zn-2.07Mg-2.42Cu alloy under peak aged (T6), over aged (T73), and retrogression and re-aged (RRA) ageing circumstances. The RRA alloy offers the best resistance to the start of fatigue cracks. The T73 sample has the biggest expansion rate and the RRA sample has the least when the stress intensity range (Δk) increases. The T6 specimen has the highest and the RRA specimen has the lowest crack-growth rates during the second stage of fracture propagation. Transgranular expansion serves as the primary foundation for the alloy's crack propagation mode under various ageing conditions. Significant secondary cracks were seen in the RRA sample, and intergranular growth was also seen in the T73 condition.

As a result of the foregoing, the aim of this work was to investigate the combined effects of heat treatments and stress ratio on the behavior of cracks developing on samples made of the cast aluminum alloy A07710 – T6 as a result of compound cyclic loads (bending-torsion). This is a particularly interesting area due to the opposite effect of aging conditions at startup and the resistance to long crack propagation.

3. EXPERIMENTAL WORK

The material of the cast aluminum alloy A07710 – T6 with the mechanical properties and chemical composition given in Tables 1 and 2 was in the form of a rolled plate. Fatigue specimens in the form of circular cross-section bars were cut with their tops parallel to the surface of the plate and their lengths aligned with the rolling direction. The two heat treatments used included the following stages [15]:

Solution treatment: 350°C 1 hr, water quenching.

Preage, 70°C 8 hrs.

Age: - either 160°C, 1 hr (underage UA) or 160°C 18 hrs (overaged OA).

Aging times were selected from a yield stress versus time aging curve at 160°C to give a (UA) and (OA) condition with the same yield strength. Long crack propagation tests were performed on single edge notch test pieces (20mm×20mm×100mm) containing central notches 5mm deep. The data of da/dN vs. ΔK were determined using Mates servo-controlled electrohydraulic testing machine operated at 50 Hz in air at 25°C. The specimens were loaded in a combined load (bending - torsion) machine test as seen in Figure 3 and the crack length was continuously monitored using a DC power source potential drop technique.

Table 1. Mechanical properties of cast aluminum alloy A07710-T6

	Tensile strength in ksi (MPa)	Yield strength in ksi (MPa)	Elongation %	Modulus of elasticity	Hardness	
					BH	VH
Standard*	≤531 MPa	≤483 MPa	≥3.0%	66.2 GPa	143	158
Measured**	42.0 (430)	32.8 (235)	4.5	68.3 GPa	141	155

Table 2.Chemical composition of cast aluminum alloy A07710-T6

	Zn	Mg	Cu	Cr	Ti	Si	Fe	Mn	Al
Standard*	≤0.10%	≤0.25%	2.4%-3.0%	≤0.05%	≤0.15%	≤0.10%	≤0.12%	≤0.05%	93.2%-95.6%
Measured**	0.11%	0.12%	1.8%	0.041%	0.14%	0.12%	0.11%	0.03%	Rem.

Note: * ASTM Standards for aluminum-American and World Standards, B221-Extruded cast rods, rods, wire, profiles and tubes [16].

** The samples were examined at the Specialized Institute for Engineering Industries-Baghdad/Iraq.

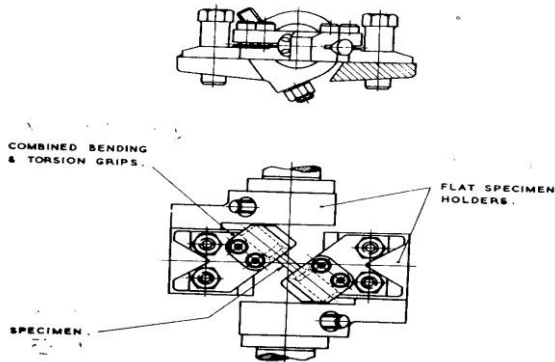


Figure 3. Combined bending - Torsion fatigue testing machine

Two types of threshold tests were performed: conventional tests at a load ratio ($R = 0.1$) where the threshold was approached by a load shedding technique with load reductions of 2% near the threshold, and constant maximum tests. In this second type of test, ΔK was reduced to the threshold by raising the minimum load while maintaining a stable maximum load. The effect of this is to increase the R ratio as ΔK falls. For these tests, the initial loads were chosen so that the threshold was reached at $R = 0.8$. Unnotched specimens in the same orientation as the notched specimen with the dimensions shown in Figure 4 were used for the short-cracking tests.

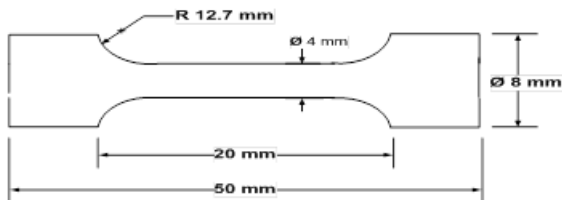


Figure 4. The geometry of combined loading fatigue specimen

The surfaces of these samples were ground and electropolished after heat treatment to ensure a smooth, stress free surface and then lightly etched. The cracks started and grew within the test area with average dimensions ($19.05 \times$

3.95ϕ)mm. A replication technique was used to keep track of crack progression, every 3500 cycles, replicas are taken. The maximum surface tension during these tests was 261MPa (90%) yield strength (σ_y).

The stress intensity values for the short crack tests were calculated using a calibration for pure bending semi-elliptical cracks [17], assuming a ratio of half surface crack length to crack depth of (0.85). This value was determined from the measurement of the crack shape for a number of cracks present on the smooth samples at the end of the tests. All cracks measured showed a similar shape under both heat treatment conditions.

4. RESULTS

4.1 Yield strength

The two conditions, UA and OA, were produced with very similar yield strength levels between 275 and 288 MPa.

4.2 Microstructure

The optical micrographs in Figures 5a and 5b illustrate the optical microstructure of the top surface of cast aluminum alloy A07710 – T₆ as a grain structure common to both aging conditions. The size of the precipitates after the two treatments can be seen in Figures 6a and 6b along with occasional ZrAl₃ dispersoid particles.

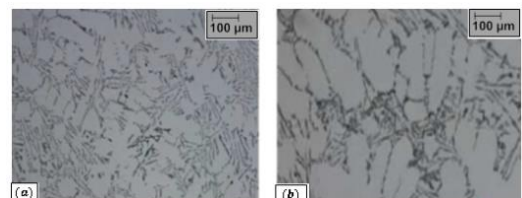


Figure 5. Optical micrographs of cast aluminium alloy A07710- T₆: (a)Top surface, (b) Short-transverse (S-T)

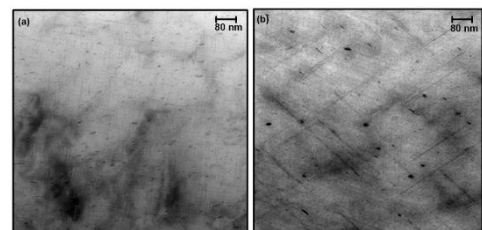


Figure 6. Transmission electron microstructure (a) Underaged (UA), (b) Overaged (OA)

4.3 Fractography

The fracture surface morphology in the area close to the threshold for longitudinal crack tests in the four combinations

of aging treatment and R-ratio is shown in Figures 7 a-d. The crack propagation is of a very similar faceted crystallographic nature in each case. Short-crack fracture surfaces are shown in Figures 7 e-f. Again, the OA and UA fracture paths are very similar and closely resemble near-threshold growth.

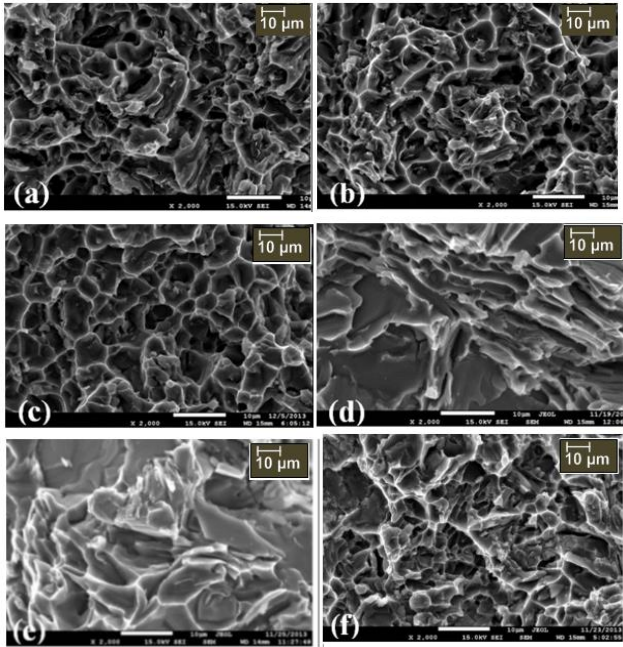


Figure 7. Near threshold fracture morphology in long crack (a) R=0.1 uperaged, (b) R=0.1 overaged, (c) R=0.8 uperaged, (d) R=0.8 overaged, short crack, (e) R=0.1 uperaged, (f) R=0.1 overaged

4.4 Fatigue crack growth

Figure 8 shows da/dN vs. ΔK for the OA state at ($R = 0.1$). The additional crack depth scale applies to the short crack results of the smooth specimen tests (filled triangles). Long crack data comes down to a threshold of approximately $2.32 \text{ MPa}\sqrt{\text{m}}$. The short crack points are for a single naturally initiated crack when cracks are deeper than $100 \mu\text{m}$, the long and short crack curves merge. Smaller cracks than these grow irregularly, but at average rates close to those of the long cracks as well as at ($R = 0.1$) ΔK values below the long crack threshold

In Figure 9, the UA material has the higher long-crack threshold of $4.68 \text{ MPa}\sqrt{\text{m}}$, although the growth rates for both conditions are very similar in the Paris regime above $8.85 \text{ MPa}\sqrt{\text{m}}$. The short crack data for the single crack in the UA material shows behavior similar to the OA, although the average growth rates are slightly lower. This is shown more clearly in Figure 10, where the scatter bands for data from three cracks in overaged specimens and two in underaged tests are indicated.

Figure 11 also shows the long crack thresholds from the constant maximum load tests. These thresholds are at R-ratios slightly above 0.8. The high R thresholds are reduced to $1.29 \text{ MPa}\sqrt{\text{m}}$ for OA and $2.09 \text{ MPa}\sqrt{\text{m}}$ for UA material.

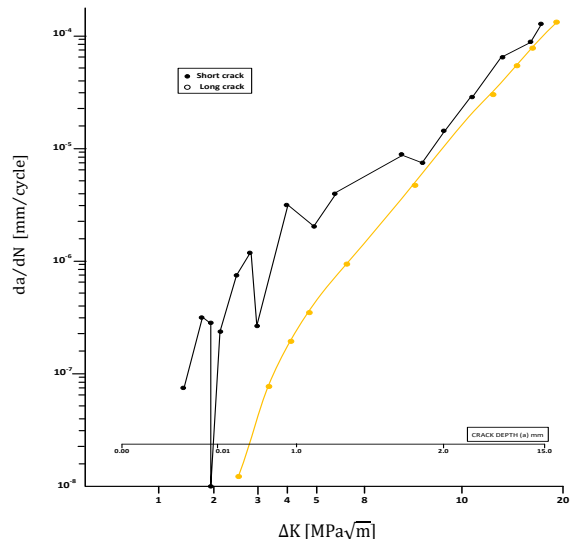


Figure 8. da/dN vs. Δk for short and long crack results of overaged alloy at 25°C & $R = 0.1$

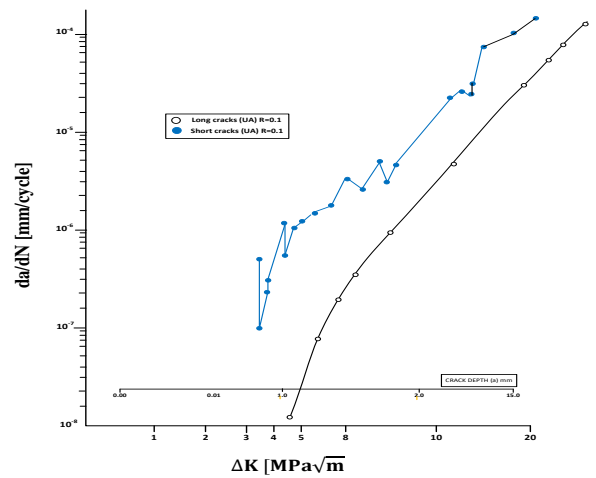


Figure 9. da/dN vs. Δk for short and long crack results of underaged alloy at 25°C & $R = 0.1$

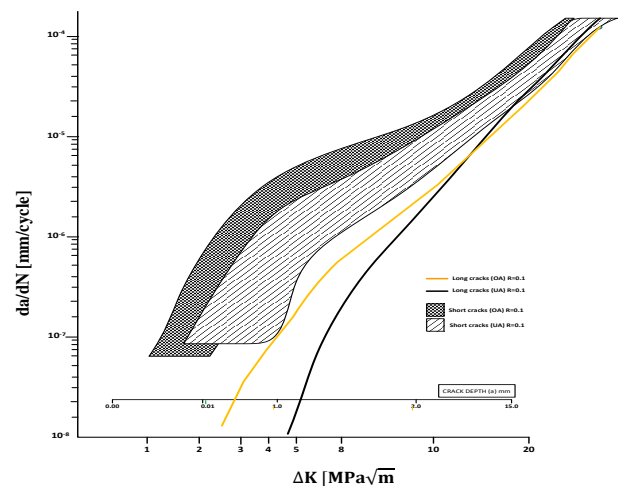


Figure 10. da/dN vs. Δk for short and long crack results of underaged alloy at 25°C & $R = 0.1$ Scatter bands for short crack data representing results from several cracks

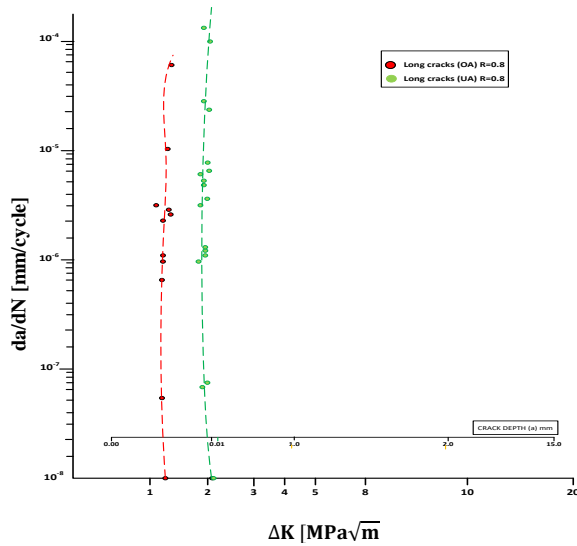


Figure 11. da/dN vs. Δk for long crack results of underaged alloy at 25°C & $R = 0.8$

5. DISCUSSION

5.1 Short crack growth

Interactions between the fracture tip and grain boundaries appear to be tightly connected to grain size, which may explain the uneven nature of short crack growth. This is clearly seen in Figure 8 for the OA material, where dips in the growth rate for the short crack occur at depths of $\approx 10, 25$ and $40 \mu\text{m}$, corresponding to the grain size between 10 and $25 \mu\text{m}$ in the S-T orientation corresponds to (Figure 5b). The resulting changes in orientation of the fracture progression at each grain boundary can be seen on the fracture surface in Figure (7f). This is consistent with many previous observations [18, 19] and has been interpreted to be due to the difficulty of reinitiating slippage in a new orientation in the next grain.

Such observations might lead to the assumption that the crack shape for the short cracks would be related to the grain shape such that cracks growing through long, thin grains would be shallow cracks with large surface length to depth ratios. However, the cracks observed here were nearly semi-circular over a wide range of crack lengths, as observed by Wang et al. [20] at crack depths of only $10 \mu\text{m}$. The consistent crack shape maintained from the first grain to the long crack regime, where the crack front spans numerous grains, suggests that it is appropriate to use a single control parameter to describe crack propagation over the full range of crack lengths. The UA condition shows better resistance to short crack propagation than the OA condition, together with the results for long cracks and in contrast to reports of resistance to crack initiation [10]. This supports the view that it is an inherent microstructural property, such as the reversibility of sliding in the plastic zone, which produces the effect.

5.2 Long crack behavior

Long-crack behavior exhibits the typical increasing threshold trend values and lower near-threshold crack growth rates in UA case than in OA case at a stress ratio $R = 0.1$ [4].

The thresholds themselves, $4.68 \text{ MPa}\sqrt{\text{m}}$ and $2.32 \text{ MPa}\sqrt{\text{m}}$, agree well with those from Maier et al. [21] work (about $4.42 \text{ MPa}\sqrt{\text{m}}$) and Antunes [22] $4.5 \text{ MPa}\sqrt{\text{m}}$ for underaged Al-Si-Mg cast alloys and $2.28 \text{ MPa}\sqrt{\text{m}}$ value for overaged alloy. Both situations' fracture surfaces near the sill are faceted, which indicates that a significant amount of asymmetric shear will be involved in the deformation of the fracture tip (Figures 7a-d). This will introduce some degree of mismatch between the two fracture faces and thus there will be a roughness-induced closure contribution to the threshold at $R = 0.1$.

Due to the wider crack apertures involved, lengthy crack behavior at high R is free from the roughness-induced closure effect [23]. Since $R = 0.1$ and $R = 0.8$ have the same fracture propagation mechanism (Figures 7 a-d), the thresholds of $R = 0.8$ can be assumed to represent intrinsic material thresholds. These match the ranges of effective stress intensities ΔK_{eff} at the tip of crack at threshold in the tests with $R = 0.1$. The recorded numbers of $2.09 \text{ MPa}\sqrt{\text{m}}$ (UA) and $2.32 \text{ MPa}\sqrt{\text{m}}$ (OA) again agree well with those of Maier et al. [20] in Al-Si-Mg cast alloys of $1.89 \text{ MPa}\sqrt{\text{m}}$ (UA) and $2.27 \text{ MPa}\sqrt{\text{m}}$ (OA). The UA has an excellent near-threshold crack propagation resistance state observed at $R = 0.1$ persists when no roughness-induced closure occurs at $R = 0.8$. This suggests that rather than a mechanical effect, such as a difference in closure behavior, this is caused by a difference in the material's inherent resistance to fatigue, including might be due to increased slip reversibility. The proposal by Maier et al. [21] that the improved toughness of UA material is due to increased crack deformation does not seem to apply in the present case since the fracture mode is very similar in both UA and OA material.

5.3 Short and long crack comparing in behavior

The propagation rates of short semi-elliptical cracks in this alloy are greater than those of long through-thickness cracks at equivalent linear elastic ΔK values and $R = 0.1$ despite a similar fracture mode (Figures 7 a-f). This observation agrees with the early work of Antunes [22] match. There has been some discussion about the improper use of short crack data from linear elastic K-plots. It is used here in conjunction with a crack depth scale for the Sime-elliptical cracks for the important reason that it shows when the cracks in the smooth specimen tests start to behave as long through-the-thickness cracks. This occurs at crack depths greater than about $100 \mu\text{m}$ under both OA and UA conditions. The grain size in the S-T orientation (Figure 5b) is between 10 and $30 \mu\text{m}$, so the crack front at this stage samples between 50 and 150 grains and gives an average of the crack growth behavior. Once the data from the two test types are merged (as shown in Figure 12), the agreement between the rates of growth of Semi-elliptical cracks and the through-thickness cracks is very good, indicating that K ranges from ≈ 9.0 to $22 \text{ MPa}\sqrt{\text{m}}$ is involved there is no influence of the crack shape on the fatigue crack propagation behavior if a suitable K calibration is used. This confirms the work of Antunes et al. [24] on the crack shape effect in 2050 – T8 aluminum alloy.

It has been hypothesized that a variation in how short and long cracks behave at low ΔK is due to not experiencing closure consequences caused by roughness when the crack is only on the order of one or two grains long [14]. It is therefore appropriate to combine short crack data with occlusion-free

long crack results, i.e. ΔK_{eff} values. This comparison can be seen in Figure 12 where long crack and high R threshold values are plotted in addition to long and short crack results at $R = 0.1$. Very little of the long crack threshold is below the short crack data at $R = 0.8$, but this is partly due to the difficulty in obtaining short crack results below a ΔK of $\approx 1.3 \text{ MPa}\sqrt{\text{m}}$ for the inclusions where the cracks initiated in the present tests were usually several microns in diameter. Obtaining such data requires further work at lower stress levels and longer test durations. Nonetheless, compared to data for long cracks without closure, very little growth of the short crack appears to be anomalously fast, suggesting that the lack of roughness-induced closure for short crack doses contributes to their high average growth rates.

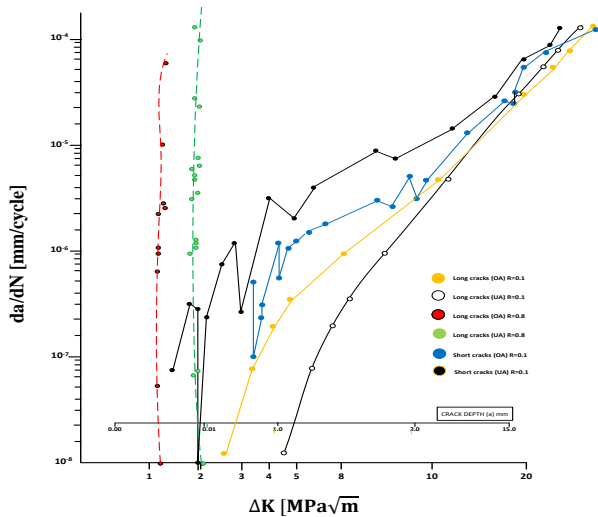


Figure 12. da/dN vs. Δk for long and short cracks results for two types of test underaged and overaged alloy $R = 0.1$ and $R = 0.8$ at 25°C

Another reason for comparing short crack results with high R long crack data is the suggestion put forward by Suzuki et al. [25] that the apparent inability of short cracks to closed even at low R lies in the extent of crack tip plasticity generated by the high top surface stresses in the short crack test - pieces. They argue that a large maximum plastic zone size is produced due to the high maximum stress combined with small reverse plastic zone because of the lack of gross yielding on unloading. Thus, it is as if the crack is growing at a high value of R compared with a simple linear elastic analysis. This should also lead to larger crack openings for short cracks than predicted from linear fracture mechanics as has been reported by Chen et al. [23].

The short crack in the smooth bend specimen is growing effectively at high R. In the Paris regime long crack data are relatively insensitive to R-ratio because of the declining importance of closure effects as symmetrical continuum deformation takes over at the crack tip and the fracture surfaces become flatter. Thus the short crack data would be expected to merge with the $R = 0.1$ long crack data in the Paris regime as the experimental results show. There may also be an additional effect in the smooth bend specimen. The effective value of R at the deepest point of the fracture may drop as it lengthens because the fiber stress in the specimen decreases as it moves away from the top surface. This would also cause the short crack data to move from the $R = 0.8$ long crack curve toward the $R = 0.1$ long crack results as

crack depth increases. This might produce a slight difference in the crack lengths at which long and short crack data merge depending on whether the short crack tests are carried out in bend.

6. CONCLUSIONS

a. Short fatigue cracks (depths) in under- and overaged cast aluminum alloy A07710 – T6 propagate faster than long through-thickness cracks simultaneously, it seemed to apply ΔK and $R = 0.1$.

b. The growth short crack rates at $R = 0.1$ correspond more closely to long crack data measured at high R than data obtained at $R = 0.1$.

c. Short and long cracks low ΔK similar faceted fracture surfaces are produced by fatigue cracks, resulting in the same crack propagation mechanism operating even if propagation speeds vary.

d. The underaged cast aluminum alloy A07710 – T6 shows better crack propagation resistance than the overaged cast aluminum alloy A07710 – T6 in both long and short crack propagation regimes. Higher long crack thresholds are obtained in the underaged cast aluminum alloy A07710 – T6, even when shuttering effects caused by roughness are eliminated.

e. Short crack growth is discontinuous and is influenced by the material's grain size.

f. Between ΔK values of ≈ 9.0 to $22 \text{ MPa}\sqrt{\text{m}}$, the crack shape has no effects on the propagation of fatigue cracks in both underaged and overaged cast aluminum alloy A07710 – T6. Semi-elliptical and continuous cracks propagate at the same rate and fracture mode in this area.

ACKNOWLEDGEMENT

The authors would like to thank the Department of Electromechanical Engineering at the University of Technology in Baghdad, Iraq for its contribution in support to carry out this work.

REFERENCES

- [1] Cai, P. (2018). A microstructure-based model validated experimentally for quantification of short fatigue crack growth in three-dimensions. Ph.D. Thesis, Department of Mechanical Engineering, University of Kentucky, UK. <https://doi.org/10.13023/etd.2018.385>
- [2] Peng, Z., Yang, S., Wang, Z., Gao, Z. (2022). Fatigue property and small crack propagation mechanism of MIGWelding joint of 6005A-T6 aluminum alloy. Materials, 15(13): 4698. <https://doi.org/10.3390/ma15134698>
- [3] Noroozi, A.H., Glinka, G., Lambert, S. (2007). A study of the stress ratio effects on fatigue crack growth using the unified two-parameter fatigue crack growth driving force. International Journal of Fatigue, 29: 1616-1633. <https://doi.org/10.1016/j.ijfatigue.2006.12.008>
- [4] Campbell, F.C. (2008). Elements of metallurgy and engineering alloys. ASM International.
- [5] Wanhill, R.J.H., Stanzl-Tschegg, S.E. (2021). Short/small fatigue crack growth, thresholds and

- environmental effects: A tale of two engineering paradigms. *Corrosion Reviews*, 39(2): 165-175. <https://doi.org/10.1515/corrrev-2020-0096>
- [6] Spangenberg, A., Gavras, A., Lados, D. (2014). Long and small fatigue crack growth in aluminum alloys. *Light Metals*, Springer, Cham. https://doi.org/10.1007/978-3-319-48144-9_48
- [7] Yoshinaka, F., Nakamura, T., Takaku, K. (2016). Effects of vacuum environment on small fatigue crack propagation in Ti-6Al-4V. *International Journal of Fatigue*, 91: 29-38. <https://doi.org/10.1016/j.ijfatigue.2016.05.024>
- [8] Wang, W., Zhang, W., Wang, H., Fang, X., Liang, X. (2016). Influence of grain boundary on the fatigue crack growth of 7050-T7451 aluminum alloy based on small time scale method. *Advances in Materials Science and Engineering*, 2016. <https://doi.org/10.1155/2016/7671530>
- [9] Liu, S., Zhu, M., Zhou, H., Wan, D., Xuan, F. (2019). Strain visualization of growing short fatigue cracks in the heat-affected zone of a Ni-Cr-Mo-V steel welded joint: Intergranular cracking and crack closure. *International Journal of Pressure Vessels and Piping*, 178: 103992. <https://doi.org/10.1016/j.ijpvp.2019.103992>
- [10] Abdullatef, M.S. (2013). Study of short cracks growth behavior for duralumin 7075-T6 Enhanced by artificial ageing as thermal and chemical treatments under rotating bending loading. *Engineering and Technology Journal*, 31(11): 2166-2182. <https://www.iasj.net/iasj/download/81fa18360f9dc768>
- [11] Pardhan, D., Mahobia, G.S., Chattopadhyay, K., Fernando, D.C., Paulose, N., Babu, S.N.N., Singh, V. (2019). Effect of stress ratio and mean stress on high cycle fatigue behavior of the superalloy IN718 at elevated temperatures. *Materials Research Express*, 6(9): 1050-1060. <http://doi.org/10.1088/2053-1591/ab3321>
- [12] Feng, R.C., Rui, Z.Y., Zuo, Y.R., Zhang, G.T., Yan, C.F. (2013). Influence of stress ratio on fatigue crack propagation in TiAl alloy. *Applied Mechanics and Materials*, 457-458. <https://doi.org/10.4028/www.scientific.net/AMM.457-458.7>
- [13] Desmukh, M.N., Pandey, R.K., Mukhopadhyay, A.K. (2006). Effect of aging treatments on the kinetics of fatigue crack growth in 7010 aluminum alloy. *Materials Science and Engineering: A*, 435-436: 318-326. <https://doi.org/10.1016/j.msea.2006.07.063>
- [14] Li, Y., Xu, G., Liu, S., Peng, X., Yin, Z., Wang, L., Liang, X. (2019). Effect of ageing treatment on fatigue crack growth of die forged Al-5.87Zn-2.07Mg-2.42Cu alloy. *Engineering Fracture Mechanics*, 215: 251-260. <https://doi.org/10.1016/j.engfracmech.2019.04.023>
- [15] Sanders, R.E. (2001). Technology innovation in aluminium products. *JOM*, 53: 21-25. <https://doi.org/10.1007/s11837-001-0115-7>
- [16] ASTM International. (2014). ASTM D5045-14: Standard test methods for plane-strain fracture toughness and strain energy release rate of plastic materials. West Conshohocken, PA: ASTM International.
- [17] Campagnolo, A., Meneghetti, G., Berto, F., Tanaka, K. (2018). Calibration of the potential drop method by means of electric FE analyses and experimental validation for a range of crack shapes. *Fatigue & Fracture of Engineering Materials & Structures*, 41(11): 2272-2285. <https://doi.org/10.1111/ffe.12856>
- [18] Jiang, H., Sandlöbes, S., Gottstein, G., Korte-Kerzel, S. (2017). On the effect of precipitates on the cyclic deformation behavior of an Al-Mg-Si alloy. *Journal of Materials Research*, 32: 4398-4410. <https://doi.org/10.1557/jmr.2017.350>
- [19] Han, W.Z., Chen, Y., Vinogradov, A., Hutchinson, C.R. (2011). Dynamic precipitation during cyclic deformation of an underaged Al-Cu alloy. *Materials Science and Engineering: A*, 528(24): 7410-7416. <https://doi.org/10.1016/j.msea.2011.06.037>
- [20] Wang, S., Xi, Y., Li, H., Bowen, P. (2019). Fractographic study on naturally initiated short fatigue cracks in a near-lamellar TiAl alloy at room temperature. *Metals*, 9(10): 1101. <https://doi.org/10.3390/met9101101>
- [21] Maier, P., Ginesta, D., Clausius, B., Hort, N. (2022). Observations of microstructure-oriented crack growth in a cast Mg-Al-Ba-Ca alloy under tension, compression and fatigue. *Metals*, 12(4): 613. <https://doi.org/10.3390/met12040613>
- [22] Antunes, F.V. (2023). Fatigue crack growth in metallic materials. *Materials*, 16(1): 11. <https://doi.org/10.3390/ma16010011>
- [23] Chen, Z., Holdsworth, S. (2018). High-R low growth rate fatigue crack propagation at elevated temperatures. *International Journal of Fatigue*, 106: 114-122. <https://doi.org/10.1016/j.ijfatigue.2017.08.020>
- [24] Antunes, F.V., Serrano, S., Branco, R., Prates, P. (2018). Fatigue crack growth in the 2050-T8 aluminium alloy. *International Journal of Fatigue*, 115: 79-88. <https://doi.org/10.1016/j.ijfatigue.2018.03.020>
- [25] Suzuki, S., Sakaguchi, M., Domen, M., Karato, T., Suzuki, K. (2022). Temperature and ΔK dependence of grain boundary effect on fatigue crack propagation in a two-dimensional polycrystalline Ni-base superalloy. *Acta Materialia*, 240. <https://doi.org/10.1016/j.actamat.2022.118288>

NOMENCLATURE

K	Stress intensity factor [$\text{MPa}\sqrt{\text{m}}$]
K_C	Critical stress intensity factor [$\text{MPa}\sqrt{\text{m}}$]
K_{Ic}	Fracture toughness [$\text{MPa}\sqrt{\text{m}}$]
ΔK_{eff}	Effective stress intensities [$\text{MPa}\sqrt{\text{m}}$]
ΔK_{appl}	Applies stress intensity factor [$\text{MPa}\sqrt{\text{m}}$]
$K_{\text{min,appl}}$	Minium applied stress intensity factor [$\text{MPa}\sqrt{\text{m}}$]
$K_{\text{max,appl}}$	Maximum applied stress intensity factor [$\text{MPa}\sqrt{\text{m}}$]
ΔK_{tot}	Total stress intensity range [$\text{MPa}\sqrt{\text{m}}$]
$K_{\text{max,tot}}$	Total maximum stress intensity factor [$\text{MPa}\sqrt{\text{m}}$]
$K_{\text{min,tot}}$	Total minimum stress intensity factor [$\text{MPa}\sqrt{\text{m}}$]
K_R	Residual stress intensity factor
da/dN	Fatigue crack length per loading cycles [mm/cycle]

C and m	Statistical constants based on material characteristics	VHCF	Very-high cycle fatigue
FCG	Fatigue crack growth	σ_{res}	Residual stress distribution
HCF	High-cycle fatigue		